electronics

MDPI

Article

Correlation between CO_2 Sensitivity and Channel-Layer Thickness in In_2O_3 Thin-Film Transistor Gas Sensors

Ayumu Nodera, Ryota Kobayashi, Tsubasa Kobayashi and Shinya Aikawa *

Department of Electrical and Electronic Engineering, Kogakuin University, Hachioji 192-0015, Tokyo, Japan
* Correspondence: aikawa@cc.kogakuin.ac.jp; Tel.: +81-42-628-4472

Abstract: CO_2 monitoring is important for achieving net-zero emissions. Here, we report on a CO_2 gas sensor based on an In_2O_3 thin-film transistor (TFT), which is expected to realize both low-temperature operation and high sensitivity. The effect of channel thickness on TFT performance is well known; however, its effect on CO_2 sensitivity has not been fully investigated. We fabricated In_2O_3 TFTs of various thicknesses to evaluate the effect of channel thickness on CO_2 sensitivity. Consequently, TFT gas sensors with thinner channels exhibited higher CO_2 sensitivity. This is because the surface effect is more prominent for a thinner film, suggesting that charge transfer between gas molecules and the channel surface through gas adsorption has a significant impact on changes in the TFT parameters in the subthreshold region. The results showed that the In_2O_3 TFT in thin channels is a promising candidate for CO_2-sensitive TFT gas sensors and is useful for understanding an effect of gas adsorption in oxide TFTs with a very thin channel as well.

Keywords: gas sensor; CO_2; In_2O_3; thin-film transistor; channel thickness

check for updates

Citation: Nodera, A.; Kobayashi, R.; Kobayashi, T.; Aikawa, S. Correlation between CO_2 Sensitivity and Channel-Layer Thickness in In_2O_3 Thin-Film Transistor Gas Sensors. *Electronics* **2024**, *13*, 1947. https://doi.org/10.3390/electronics13101947

Academic Editors: Jae-Hyung Jang, Tao Wang, Frédérique Ducroquet, Yi Gu and Hongtao Li

Received: 30 March 2024
Revised: 7 May 2024
Accepted: 14 May 2024
Published: 16 May 2024

1. Introduction

CO_2 monitoring is important in many industries, including petrochemicals, combustion control, medicine, agriculture, food, and chemical plants, as well as in terms of the environment [1,2], and is currently required to achieve net-zero emissions. Therefore, the demand for CO_2 gas sensors has increased in many applications. Although several studies have reported on CO_2 detection methods [3], semiconductor gas sensors are expected to become one of the most important electronic devices that can achieve sustainable development owing to their small size, high sensitivity, relatively easy fabrication, and low power consumption [4].

The most typical semiconductor gas sensor is the two-terminal type. An advantage of this type of sensor is its facile fabrication owing to its simple configuration. When gas molecules are adsorbed onto oxide semiconductor surfaces and grain boundaries, charge transfer occurs at the interfaces, resulting in the formation of a depletion layer or potential barrier. The change in its electrical resistance due to charge transfer indicates the presence of gas molecules [5]. Because reducing gases such as NO and CO are highly reactive, the electrical conductivity changes significantly due to charge transfer from the semiconductor surface [6]. However, some difficulties persist in terms of CO_2 detection because CO_2 is chemically stable. As a result, thermal assistance is generally required to activate charge transfer. Therefore, sensitivity enhancement of CO_2 detection has been performed by introducing basic oxides such as CaO and La_2O_3 into oxide semiconductors [7–9] or by increasing the adsorption surface area using nanomaterials [10,11]. However, because the operating temperature is 300 °C or higher, achieving both a lower operating temperature and higher sensitivity is difficult.

A highly sensitive semiconductor gas sensor using a transistor structure has been proposed to address this issue. Such a sensor detects gases by changing its parameters in the subthreshold region; therefore, it is capable of highly sensitive detection of trace gases

and operates at low temperatures. CO_2 sensing at relatively low operating temperatures has been reported using ionic electrolytes [12,13] and a GaN-based high-electron-mobility transistor (HEMT) [14,15]. However, these structures and fabrication processes are very complex. For example, with ionic electrolytes, it is very hard to integrate sensor components. An HEMT is an important part of a chip sensor and has been widely used for gas sensor application, but the off-state current is rather high. This is not good for realization of a low-power-consumption integrated circuit (IC). On the other hand, an oxide thin-film transistor (TFT) without a passivation layer structure in which the surface of the semiconductor channel is exposed to the atmosphere has been proposed for gas sensor application [16,17]. Oxide TFTs show a low off-state current and have a very simple structure, possibly leading to the realization of low-power-consumption sensor ICs.

Although many oxide semiconductors for TFTs have been developed, In_2O_3-based materials whose electrical properties change depending on the surrounding atmosphere are suitable for the active channel of such TFT sensors [18,19], and actual sensing of gases such as NO_x and H_2 has been reported [20–22]. Recently, review papers on In_2O_3 transistor-based gas sensors have been published overviewing their history, working principles, synthesis, and future applications [23,24]. Paghi et al. summarized a gas sensor based on an In_2O_3 nanowire field-effect transistor, which can serve a large reaction surface compared to a flat and smooth semiconductor device. Shah et al. also proposed nanostructured In_2O_3 lending an advantage to gas sensor applications. Thanks to the large surface area, good prospects in trace-gas detection are expected. CO_2 sensing with high sensitivity, however, is still difficult using a transistor-type gas sensor not only in nanostructured In_2O_3 but also other oxide TFTs such as SnO_2 and ZnO [25,26]. Under these circumstances, we demonstrated CO_2 detection using In_2O_3 TFT at a relatively low operating temperature of 150 °C, focusing on the crystal structure of the channel surface [27]. We previously reported that in addition to the effect of the measurement environment on TFT characteristics, O^{2-} and H^+ impurities incorporated in the film induce a degradation in electron conduction, and this increases with an increase in the film thickness [28]. Gao et al. estimated the degradation tendency of intrinsic mobility and subthreshold slope with an increase in the film thickness [29]. This trend is affected by the measurement environment, and while the fluctuations are noticeable in vacuum with small amounts of surface-adsorbed gases, they are small in an atmospheric environment. In other words, the dependence of TFT parameters on film thickness owing to the measurement environment is an important factor that needs to be clarified for TFT gas sensors. In this study, we fabricated an open-channel-type TFT with a back-gate structure using various In_2O_3 channel thicknesses and examined the correlation between the channel thickness and CO_2 gas sensitivity.

2. Device Fabrication and Characterization

A bottom-gate TFT was fabricated on a Si substrate with a 200 nm-thick thermally grown oxide layer. Before the deposition of the active channel, the substrate was ultrasonically cleaned in acetone and isopropyl alcohol and irradiated using an excimer lamp (wavelength: 172 nm) for 15 min to remove any organic residue. The In_2O_3 channel was deposited via RF magnetron sputtering at room temperature using a 4N-purity, 3-inch-diameter In_2O_3 ceramic target. The thickness of the active channel formed through a stencil shadow mask in the range of 5–50 nm was adjusted by varying the deposition time. The film thickness was measured using a surface profilometer (Dektak XT-E). The $O_2/(Ar + O_2)$ ratio, RF power, and working pressure were fixed at 25%, 50 W, and 0.24 Pa, respectively. The background pressure was evacuated to less than ~4×10^{-4} Pa. Subsequently, Cu-source and drain electrodes (t = 150 nm) were deposited via electron-beam evaporation through a stencil shadow mask. The channel width (W) and the length (L) were fixed at 1000 μm and 350 μm, respectively. Subsequently, the as-deposited In_2O_3 TFTs were annealed at 150 °C in air for 30 min. The binding states of the In_2O_3 film were analyzed by XPS (JEOL JPS-9030, Tokyo, Japan) with Mg Kα radiation (1.2536 keV), and the XPS

spectrum was calibrated using the C 1*s* peaks (284.6 eV) from amorphous hydrocarbon contamination of the sample surface.

The fabricated TFT sensor was characterized in a vacuum probe station under an inert N_2 atmosphere, which was then replaced with a CO_2 atmosphere. The sensor was heated at 150 °C during measurement using perfluoropolyether heat-transfer fluid (Galden HT-200, Solvay Specialty Polymers, Bollate, Italy), and all environments were at atmospheric pressure during the characterization of the gas sensitivity. The current–voltage (*I*–*V*) characteristics of the fabricated TFTs were measured using a semiconductor parameter analyzer (Agilent 4156A, Santa Clara, CA, USA). A schematic cross-sectional diagram of the TFT and setup are shown in Figure 1.

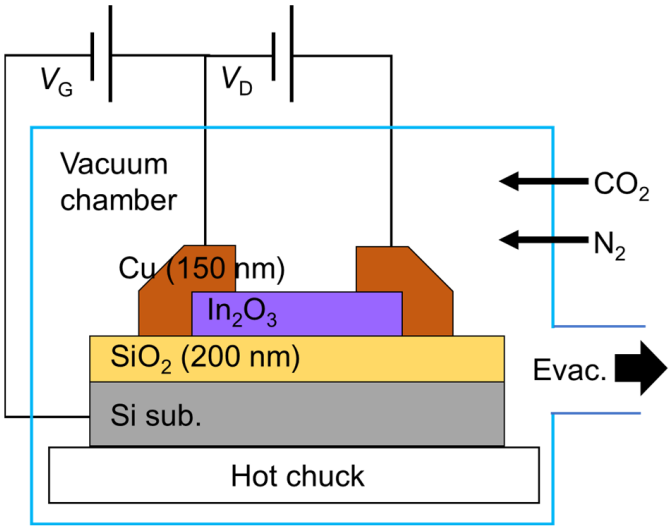

Figure 1. Schematic diagram of fabricated TFT and measurement setup.

3. Results and Discussion

3.1. Channel Thickness-Dependent Transfer Characteristics at Room Temperature

Figure 2 shows the channel thickness-dependent transfer characteristics of In_2O_3 TFTs. The maximum drain current ($I_{D,max}$) increases with a decrease in the thickness. In general, surface and interface scattering become more prominent with a decrease in the channel thickness, thereby decreasing the mobility [30,31]. However, in this study, $I_{D,max}$ increased and threshold voltage (V_{th}) shifted negatively with a decrease in the thickness. The degradation of $I_{D,max}$ is possibly due to the decreased carrier concentration caused by the positively charged ions incorporated in the In_2O_3 channel. In magnetron sputtering, which uses non-equilibrium reactions, the unintentional incorporation of unwanted ions such as Ar^+ has been reported [32–34], and the number of positively charged ions in the film increases with an increase in the film thickness [35]. Then, the ions recombine with electrons, resulting in decreased carrier concentration. In other words, the increase in $I_{D,max}$ with a decrease in the film thickness can be considered to indicate that the carrier concentration is getting closer to an original intrinsic carrier density. The negative shift of the V_{th} is thus reasonably understood by an increase in carrier concentration. The reason that the anormal phenomenon of contradictory relationship between channel thickness and V_{th} might come from the short target-substrate distance of our sputtering system [36], which could incorporate large number of impurities during sputtering deposition. Because carrier concentration of the channel strongly influences the TFT performance, this is a significant finding that is directly related to the sensitivity of gas sensor devices that utilize charge transfer between the channel surface and adsorbed gas molecules.

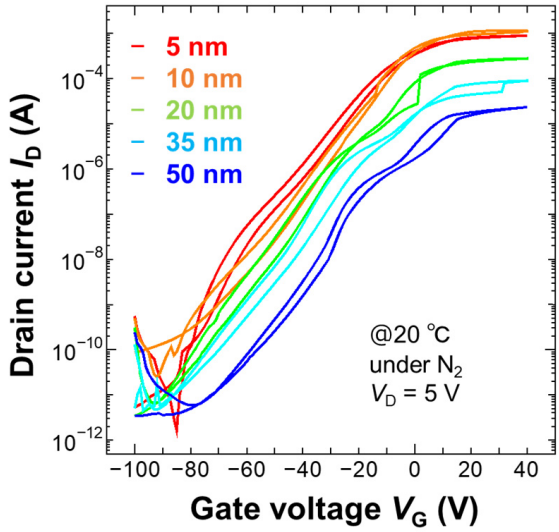

Figure 2. Thickness-dependent transfer characteristics of In_2O_3 TFTs at room temperature.

3.2. Typical Transfer Characteristics of In_2O_3 TFTs under N_2 and CO_2 Atmosphere

In semiconductor gas sensors, the surface is activated by heating during measurement to enhance reactivity with the surrounding gas [6]. However, the electrical properties of In_2O_3 TFTs change significantly depending on the measurement temperature [37]. To examine the temperature dependence of TFT properties, we varied the stage temperature from room temperature (20 °C) to 150 °C and measured the TFT properties. Figure 3 shows the temperature-dependent transfer characteristics of the In_2O_3 TFT under an inert N_2 atmosphere. In this case, we focused on the 5 nm-thick TFT. Other TFTs also showed the same tendency. To compare the characteristics at each measurement temperature, a series of TFT parameters, i.e., V_{th}, on- and off-state current ratio (I_{on}/I_{off}), subthreshold swing (SS), and field-effect mobility in the linear regime (μ_{FE}), were estimated. V_{th} is defined as the intersection point of the horizontal axis and the tangential line drawn from the point of maximum slope in the linear transfer characteristics in Figure 3a. I_{on}/I_{off} was extracted from the ratio of the on-state current (maximum I_D) and off-state current (minimum I_D) in Figure 3b. SS and μ_{FE} were computed using the following equations [38–40]:

$$SS = \left(\frac{\partial \log_{10} I_D}{\partial V_G}\right)^{-1} \quad (1)$$

$$\mu_{FE} = \frac{\partial I_D}{\partial V_G}\frac{L}{W}\frac{1}{C_i V_D}, \quad (2)$$

where V_G and V_D are the gate and drain voltage, respectively, L and W are the channel length and width, respectively, and C_i is the gate capacitance per unit area, which in this case is estimated to be 1.73×10^{-8} F/cm^2 based on a dielectric constant of 3.9 for SiO_2. As the temperature increased, V_{th} shifted in a negative direction and the I_{on}/I_{off} and SS deteriorated (Table 1).

Figure 4 shows the XPS spectrum of the O 1s core level in the In_2O_3 thin film (t = 100 nm). The background due to inelastically scattered electrons was subtracted using the Shirley method. Generally, the O 1s spectrum of In_2O_3 can be deconvoluted into three peaks at 529.5, 530.6, and 531.8 eV, which are assigned to the In-O bonds on metal oxides (M-O), an oxygen-deficient region (related to the V_O), and chemisorbed OH^- species on the surface (M-OH), respectively [41]. The estimated peak area ratio for M-O, V_O and M-OH is 74.12%, 14.63%, and 11.25%, respectively. However, a slight downshift of ~0.5 eV for the M-O component was observed in our In_2O_3. This shift is possibly caused by electron transfer [42], resulting in decreased carrier density compared to the standard In_2O_3. As we mentioned above, our oxide films may incorporate Ar^+ impurities, and they cause a decrease in carrier concentration. The XPS result therefore indicates ion impurities incor-

porated during sputtering capture of electrons in the film. In an In_2O_3 semiconductor, oxygen vacancies (V_O) are easily created [43,44] and form both shallow donor and deep trap levels [38]. Thermally activated electrons can transition from deep-level trap sites to the conduction band [45]. Therefore, the deterioration in electrical properties with an increase in temperature is caused by the activation of V_O-derived electrons, which increases the carrier density.

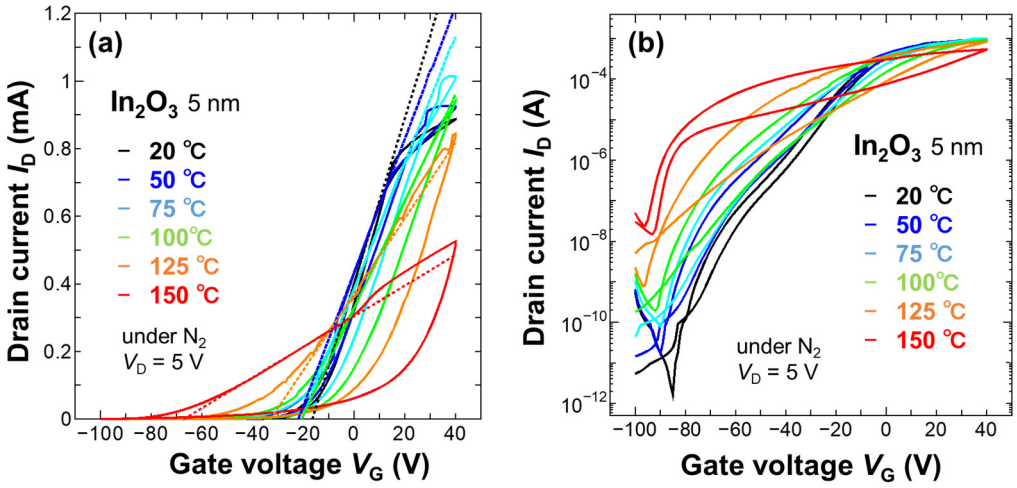

Figure 3. Temperature-dependent transfer characteristics of the 5 nm-thick In_2O_3 TFT: (**a**) linear and (**b**) semi-logarithmic plots. Measurements were performed under a N_2 atmosphere.

Table 1. Extracted V_{th}, I_{on}/I_{off}, SS, and μ_{FE} for In_2O_3 TFTs with a thickness of 5 nm, which were measured at different temperatures.

Temperature (°C)	V_{th} (V)	I_{on}/I_{off}	SS (V/dec)	μ_{FE} (cm^2/Vs)
20	−16.4	5.4×10^8	1.28	98.9
50	−21.9	5.6×10^7	2.33	80.0
75	−20.5	1.3×10^7	3.53	75.8
100	−20.6	4.9×10^5	3.18	64.2
125	−32.8	1.1×10^6	3.41	45.4
150	−67.0	4.8×10^4	3.59	18.3

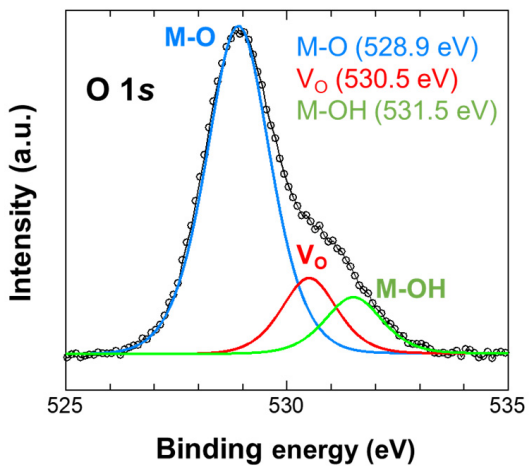

Figure 4. Typical XPS spectrum of O 1*s* core level in the In_2O_3 thin film. The open circles are the obtained raw data, and the solid black line is the best-fitted result. The peak fitting was performed using the pseudo-Voigt function.

Because the fabricated In_2O_3 TFT exhibited on/off behavior even when it was heated to 150 °C, we measured the transfer characteristics under different N_2 and CO_2 atmospheres, as shown in Figure 5. A decrease in the off-current was confirmed under a CO_2 atmosphere, indicating CO_2 detection. Because the decrease in the current exhibited a gate-voltage dependence, we plotted the current reduction ratio as a function of the gate voltage. Figure 6 shows the relationships between CO_2 sensitivity and gate voltage and between the *SS* value under a N_2 atmosphere and gate voltage. The CO_2 sensitivity was estimated from the ratio of I_D under N_2 (I_{N2}) and CO_2 (I_{CO2}) atmospheres. The highest CO_2 sensitivity was obtained in the subthreshold region of the small *SS* value. Although the operating temperature of the TFT-type CO_2 sensor we fabricated still needs thermal activation, lowering the temperature should be considered for future application. Singh and Zou proposed that functionalization of the In_2O_3 surface with metal nanoparticles is effective in enhancing gas sensitivity, achieving room temperature sensing [46,47]. Thus, functionalization will be an efficient direction for further reducing energy consumption for In_2O_3 TFT-based CO_2 sensors.

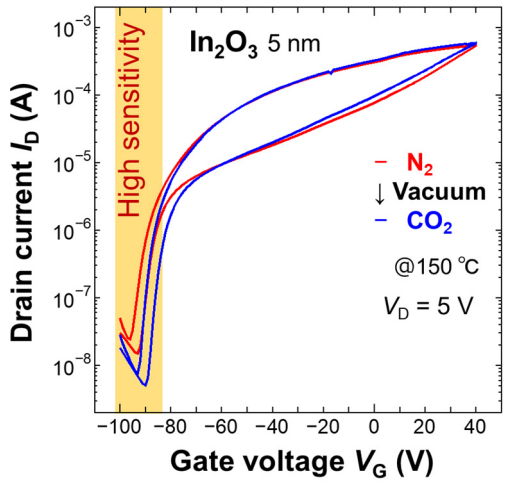

Figure 5. Transfer characteristics of the 5 nm-thick In_2O_3 TFT under N_2 and CO_2.

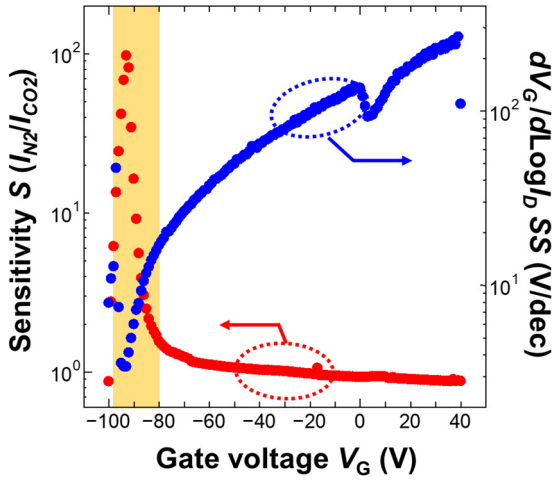

Figure 6. Sensitivity (red) and *SS* values (blue) of the 5 nm-thick In_2O_3 TFT as a function of gate voltage.

3.3. TFT Channel Thickness-Dependent CO_2 Sensitivity

Figure 7 shows the CO_2 sensitivity of the In_2O_3 TFT as a function of channel thickness. Each sensitivity was extracted from the maximum value of the V_G-dependent plot (Figure 6 for the case of the 5 nm-thick TFT). The CO_2 sensitivity increased as film thickness decreased;

the maximum sensitivity was obtained at 5 nm. We believe that the formation of a depletion layer reaches the backchannel surface owing to the thinning of the film even at 150 °C [48]. As we discussed, V_{th} was shifted under heating, which is more remarkable in thicker films, with less on/off behavior. However, the 5 nm-thick TFT retained its switching behavior, suggesting that the channel depletes even at 150 °C. A slight improvement in sensitivity in the 50 nm-thick TFT might be due to increased surface roughness. It is well known that crystallinity in In_2O_3 can be converted to polycrystalline from smooth-surfaced amorphous layers of with increasing thickness [49].

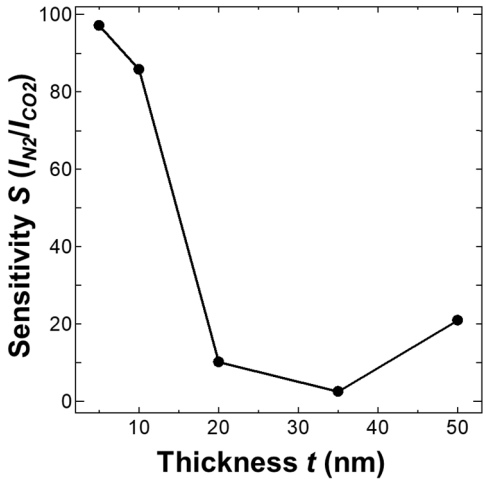

Figure 7. Relationship between sensitivity and thickness of the In_2O_3 TFT.

Figure 8 shows a schematic of the sensing mechanism to examine this tendency. In the initial state, where the gate voltage was 0 V, no electric field was applied; therefore, the overall film was in a neutral region in the semiconductor state (Figure 8a). Subsequently, when CO_2 gas was introduced, CO_2 molecules were adsorbed onto the surface and captured electrons from the semiconductor, forming CO_2^-, as indicated in the following reaction [6,50].

$$CO_2 + e^- \rightarrow CO_2^- \quad (3)$$

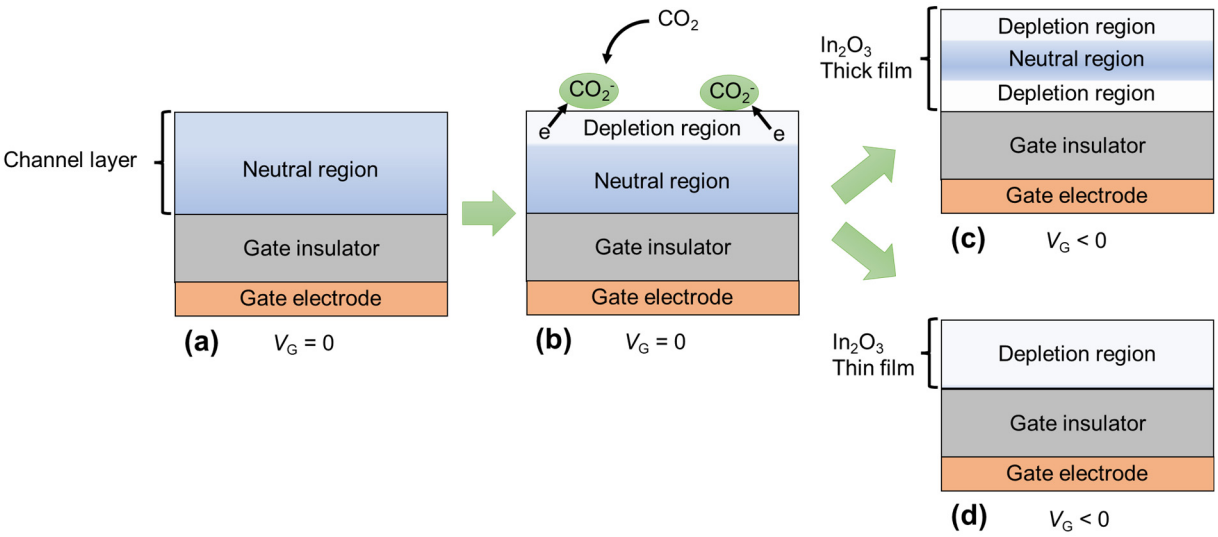

Figure 8. Schematic diagram of sensing mechanism: (**a**) initial state after fabrication; (**b**) adsorption of CO_2 molecules; (**c**) in thick channels, the neutral region is retained; (**d**) in thin channels, the whole channel layer is fully depleted.

Charge transfer occurs at the surface of the channel owing to the adsorption of CO_2 molecules, forming a depletion layer. Even in oxide semiconductors such as InGaZnO, electron traps formed by adsorbed molecules contribute to the formation of a surface depletion layer [5,51,52]. It can be inferred that a similar phenomenon occurs because of CO_2 adsorption, which acts as an acceptor (Figure 8b).

The depletion layer formed on the surface affects the subthreshold region of the TFT. When a negative gate voltage was applied, a depletion layer was formed at the In_2O_3–SiO_2 interface. However, if the channel was a thick film, the distance from the surface to the In_2O_3–SiO_2 interface was long; therefore, a neutral region remained in the middle part (Figure 8c). On the other hand, the distance decreased in the thin-channel case, and hence the overall channel was depleted (Figure 8d). In other words, in thick films, the effect of the surface depletion layer is small. However, in thin films, the surface depletion layer causes a transition to the subthreshold region at a smaller V_G. This phenomenon directly improves the sensitivity of the gas sensor because, as mentioned above, for gas sensing in TFTs that utilize charge transfer with the adsorbed gas molecules, a shift in V_{th} correlates with a change in the carrier density in the depletion layer region [53]. Therefore, after CO_2 adsorption, V_{th} shifted slightly in the positive direction (Figure 6) and CO_2 sensitivity increased in the *SS* region, where a depletion layer was formed. In terms of the film thickness, the surface state became more sensitive as the film thickness decreased, and the highest CO_2 sensitivity was obtained in the case of the thinnest-channel TFT.

4. Conclusions

We fabricated In_2O_3 TFTs with different channel-layer thicknesses and evaluated their CO_2 sensitivity at 150 °C. The $I_{D,max}$ increased and V_{th} negatively shifted as the thickness decreased, possibly due to the decrease in the carrier concentration in the In_2O_3 film. We plotted the relationship between CO_2 sensitivity and the thickness of the In_2O_3 TFT based on the thickness-dependent TFT properties. The 5 nm-thick TFT exhibited the highest CO_2 sensitivity. This is because for a thinner film, the active channel can be fully depleted at a smaller V_G owing to charge transfer to the adsorbed molecules. In addition, TFT characterization under N_2 and CO_2 atmospheres indicates that CO_2 sensitivity depends on the applied gate voltage, as higher sensitivity was obtained in the subthreshold region. These findings suggest that In_2O_3 in thin channels is a promising candidate for CO_2-sensitive TFT gas sensors and is useful for realization of high-performance atomically thin In_2O_3 TFTs.

Author Contributions: S.A. conceived the concept and designed the experiments. A.N. performed TFT fabrication and characterization. R.K. supported TFT fabrication. T.K. supported film characterization. S.A. and A.N. performed data analysis and wrote the paper. All authors have read and agreed to the published version of the manuscript.

Funding: This study was funded in part by JSPS KAKENHI (grant 22K04932).

Data Availability Statement: The data that support the findings of this study are available from the corresponding author upon reasonable request.

Acknowledgments: The thin-film analyses and TFT fabrication were performed at the Functional Microstructured Surface Research Center of Kogakuin University. We acknowledge Masatoshi Ito of Kogakuin University for providing access to clean-room facilities and thank Kanta Kibishi and Shinri Yamadera for fruitful discussions.

Conflicts of Interest: The authors declare no conflicts of interest.

References

1. Lin, Y.; Fan, Z. Compositing strategies to enhance the performance of chemiresistive CO_2 gas sensors. *Mater. Sci. Semicond. Process.* **2020**, *107*, 104820. [CrossRef]
2. Dhall, S.; Mehta, B.; Tyagi, A.; Sood, K. A review on environmental gas sensors: Materials and technologies. *Sens. Int.* **2021**, *2*, 100116. [CrossRef]
3. Neethirajan, S.; Jayas, D.S.; Sadistap, S. Carbon Dioxide (CO_2) Sensors for the Agri-food Industry—A Review. *Food Bioprocess Technol.* **2009**, *2*, 115–121. [CrossRef]

4. Suh, J.-H.; Cho, I.; Kang, K.; Kweon, S.-J.; Lee, M.; Yoo, H.-J.; Park, I. Fully integrated and portable semiconductor-type multi-gas sensing module for IoT applications. *Sens. Actuators B* **2018**, *265*, 660–667. [CrossRef]
5. Dey, A. Semiconductor metal oxide gas sensors: A review. *Mater. Sci. Eng. B* **2018**, *229*, 206–217. [CrossRef]
6. Shankar, P.; Rayappan, J.B.B. Gas sensing mechanism of metal oxides: The role of ambient atmosphere, type of semiconductor and gases—A review. *Sci. Lett.* **2015**, *4*, 126.
7. Prim, A.; Pellicer, E.; Rossinyol, E.; Peiró, F.; Cornet, A.; Morante, J.R. A Novel Mesoporous CaO-Loaded In_2O_3 Material for CO_2 Sensing. *Adv. Funct. Mater.* **2007**, *17*, 2957–2963. [CrossRef]
8. Ehsani, M.; Hamidon, M.N.; Toudeshki, A.; Abadi, M.H.S.; Rezaeian, S. CO_2 Gas Sensing Properties of Screen-Printed La_2O_3/SnO_2 Thick Film. *IEEE Sens. J.* **2016**, *16*, 6839–6845. [CrossRef]
9. Ghosh, A.; Zhang, C.; Zhang, H.; Shi, S. CO_2 Sensing Behavior of Calcium-Doped ZnO Thin Film: A Study To Address the Cross-Sensitivity of CO_2 in H_2 and CO Environment. *Langmuir* **2019**, *35*, 10267–10275. [CrossRef]
10. Hassan, H.S.; Kashyout, A.; Morsi, I.; Nasser, A.; Ali, I. Synthesis, characterization and fabrication of gas sensor devices using ZnO and ZnO: In nanomaterials. *Beni-Suef Univ. J. Basic Appl. Sci.* **2014**, *3*, 216–221.
11. Steinhauer, S. Gas sensors based on copper oxide nanomaterials: A review. *Chemosensors* **2021**, *9*, 51. [CrossRef]
12. Wu, M.; Shin, J.; Hong, Y.; Jang, D.; Jin, X.; Kwon, H.-I.; Lee, J.-H. An FET-type gas sensor with a sodium ion conducting solid electrolyte for CO_2 detection. *Sens. Actuators B* **2018**, *259*, 1058–1065. [CrossRef]
13. Ersoez, B.; Schmitt, K.; Wöllenstein, J. Electrolyte-gated transistor for CO_2 gas detection at room temperature. *Sens. Actuators B* **2020**, *317*, 128201. [CrossRef]
14. Chang, C.; Kang, B.; Wang, H.; Ren, F.; Wang, Y.; Pearton, S.; Dennis, D.; Johnson, J.; Rajagopal, P.; Roberts, J. CO_2 detection using polyethylenimine/starch functionalized AlGaN/GaN high electron mobility transistors. *Appl. Phys. Lett.* **2008**, *92*, 232102. [CrossRef]
15. Ťapajna, M.; Simms, R.J.; Pei, Y.; Mishra, U.K.; Kuball, M. Integrated optical and electrical analysis: Identifying location and properties of traps in AlGaN/GaN HEMTs during electrical stress. *IEEE Electron Device Lett.* **2010**, *31*, 662–664. [CrossRef]
16. Hong, S.; Wu, M.; Hong, Y.; Jeong, Y.; Jung, G.; Shin, W.; Park, J.; Kim, D.; Jang, D.; Lee, J.-H. FET-type gas sensors: A review. *Sens. Actuators B* **2021**, *330*, 129240. [CrossRef]
17. Singh, A.; Chowdhury, N.; Roy, S.C.; Bhowmik, B. Review of Thin Film Transistor Gas Sensors: Comparison with Resistive and Capacitive Sensors. *J. Electron. Mater.* **2022**, *51*, 1974–2003. [CrossRef]
18. Ide, K.; Kikuchi, Y.; Nomura, K.; Kimura, M.; Kamiya, T.; Hosono, H. Effects of excess oxygen on operation characteristics of amorphous In-Ga-Zn-O thin-film transistors. *Appl. Phys. Lett.* **2011**, *99*, 093507. [CrossRef]
19. Aikawa, S.; Mitoma, N.; Kizu, T.; Nabatame, T.; Tsukagoshi, K. Suppression of excess oxygen for environmentally stable amorphous In-Si-O thin-film transistors. *Appl. Phys. Lett.* **2015**, *106*, 192103. [CrossRef]
20. Kim, K.S.; Ahn, C.H.; Jung, S.H.; Cho, S.W.; Cho, H.K. Toward Adequate Operation of Amorphous Oxide Thin-Film Transistors for Low-Concentration Gas Detection. *ACS Appl. Mater. Interfaces* **2018**, *10*, 10185–10193. [CrossRef] [PubMed]
21. Li, B.; Lai, P.T.; Tang, W.M. Hydrogen Sensors Based on TFTs with Catalytic Source/Drain Electrodes: IGZO Versus Pentacene. *IEEE Electron Device Lett.* **2018**, *39*, 1596–1599.
22. Vijjapu, M.T.; Surya, S.; Zalte, M.; Yuvaraja, S.; Baghini, M.S.; Salama, K.N. Towards a low cost fully integrated IGZO TFT NO_2 detection and quantification: A solution-processed approach. *Sens. Actuators B* **2021**, *331*, 129450. [CrossRef]
23. Paghi, A.; Mariani, S.; Barillaro, G. 1D and 2D Field Effect Transistors in Gas Sensing: A Comprehensive Review. *Small* **2023**, *19*, 2206100. [CrossRef] [PubMed]
24. Shah, S.; Hussain, S.; Din, S.T.U.; Shahid, A.; Amu-Darko, J.N.O.; Wang, M.; Tianyan, Y.; Liu, G.; Qiao, G. A Review on In_2O_3 Nanostructures for Gas Sensing Applications. *J. Environ. Chem. Eng.* **2024**, *12*, 112538. [CrossRef]
25. Hong, Y.; Kim, C.-H.; Shin, J.; Kim, K.Y.; Kim, J.S.; Hwang, C.S.; Lee, J.-H. Highly selective ZnO gas sensor based on MOSFET having a horizontal floating-gate. *Sens. Actuators B* **2016**, *232*, 653–659. [CrossRef]
26. Jeong, H.-S.; Park, M.-J.; Kwon, S.-H.; Joo, H.-J.; Kwon, H.-I. Highly sensitive and selective room-temperature NO_2 gas-sensing characteristics of SnO_X-based p-type thin-film transistor. *Sens. Actuators B* **2019**, *288*, 625–633. [CrossRef]
27. Nodera, A.; Aikawa, S. In_2O_3-based thin-film transistors with a (400) polar surface for CO_2 gas detection at 150 °C. *Mater. Sci. Eng. B* **2024**, *299*, 117034. [CrossRef]
28. Nakamura, K.; Sasaki, K.; Aikawa, S. Gas adsorption effects on electrical properties of amorphous In_2O_3 thin-film transistors under various environments. *Jpn. J. Appl. Phys.* **2020**, *59*, SIIG06. [CrossRef]
29. Gao, X.; Lin, M.-F.; Mao, B.-H.; Shimizu, M.; Mitoma, N.; Kizu, T.; Ou-Yang, W.; Nabatame, T.; Liu, Z.; Tsukagoshi, K. Correlation between active layer thickness and ambient gas stability in IGZO thin-film transistors. *J. Phys. D Appl. Phys.* **2016**, *50*, 025102. [CrossRef]
30. Noh, J.H.; Ryu, S.Y.; Jo, S.J.; Kim, C.S.; Sohn, S.-W.; Rack, P.D.; Kim, D.-J.; Baik, H.K. Indium oxide thin-film transistors fabricated by RF sputtering at room temperature. *IEEE Electron Device Lett.* **2010**, *31*, 567–569.
31. Lee, S.Y.; Kim, D.H.; Chong, E.; Jeon, Y.W.; Kim, D.H. Effect of channel thickness on density of states in amorphous InGaZnO thin film transistor. *Appl. Phys. Lett.* **2011**, *98*, 122105. [CrossRef]
32. Nomoto, J.; Makino, H.; Inaba, K.; Kobayashi, S.; Yamamoto, T. Effects of the erosion zone of magnetron sputtering targets on the spatial distribution of structural and electrical properties of transparent conductive Al-doped ZnO polycrystalline films. *J. Appl. Phys.* **2018**, *124*, 065304. [CrossRef]

33. Nomoto, J.; Makino, H.; Nakajima, T.; Tsuchiya, T.; Yamamoto, T. Improvement of the properties of direct-current magnetron-sputtered Al-doped ZnO polycrystalline films containing retained Ar atoms using 10-nm-thick buffer layers. *ACS Omega* **2019**, *4*, 14526–14536. [CrossRef] [PubMed]
34. Nomoto, J.; Nakajima, T.; Yamaguchi, I.; Tsuchiya, T. Influence of unintentionally incorporated Ar atoms on the crystalline polarity of magnetron-sputtered Al-doped ZnO polycrystalline films on glass and sapphire substrates. *J. Vac. Sci. Technol. B* **2020**, *38*, 022202. [CrossRef]
35. Barquinha, P.; Pimentel, A.; Marques, A.; Pereira, L.; Martins, R.; Fortunato, E. Influence of the semiconductor thickness on the electrical properties of transparent TFTs based on indium zinc oxide. *J. Non-Cryst. Solids* **2006**, *352*, 1749–1752. [CrossRef]
36. Aikawa, S.; Shibata, Y.; Morinaga, Y. B-doped In_2O_3 Transparent Electrode for Si-based Schottky Barrier Solar Cell Application. In Proceedings of the 2020 IEEE 20th International Conference on Nanotechnology (IEEE-NANO), Virtual, 29–31 July 2020; pp. 202–206.
37. Charnas, A.; Lin, Z.; Zhang, Z.; Ye, P.D. Atomically thin In_2O_3 field-effect transistors with 10^{17} current on/off ratio. *Appl. Phys. Lett.* **2021**, *119*, 263503. [CrossRef]
38. Kamiya, T.; Nomura, K.; Hosono, H. Present status of amorphous In-Ga-Zn-O thin-film transistors. *Sci. Technol. Adv. Mater.* **2010**, *11*, 044305. [CrossRef] [PubMed]
39. Sze, S.M.; Ng, K.K. *Physics of Semiconductor Devices*; John Wiley & Sons: Hoboken, NJ, USA, 2006.
40. Kagan, C.R.; Andry, P. *Thin-Film Transistors*; CRC Press: Boca Raton, FL, USA, 2003.
41. Donley, C.; Dunphy, D.; Paine, D.; Carter, C.; Nebesny, K.; Lee, P.; Alloway, D.; Armstrong, N.R. Characterization of Indium− Tin oxide interfaces using X-ray photoelectron spectroscopy and redox processes of a chemisorbed probe molecule: Effect of surface pretreatment conditions. *Langmuir* **2002**, *18*, 450–457. [CrossRef]
42. Watanabe, K.; Kawaguchi, T.; Aikawa, S. p-type conversion of distorted SnO_x thin film by mild thermal annealing treatment in pure N_2 environment. *AIP Adv.* **2022**, *12*, 105102. [CrossRef]
43. Aikawa, S.; Nabatame, T.; Tsukagoshi, K. Effects of dopants in InO_x-based amorphous oxide semiconductors for thin-film transistor applications. *Appl. Phys. Lett.* **2013**, *103*, 172105. [CrossRef]
44. Aikawa, S.; Nabatame, T.; Tsukagoshi, K. Si-incorporated amorphous indium oxide thin-film transistors. *Jpn. J. Appl. Phys.* **2019**, *58*, 090506. [CrossRef]
45. Ding, X.; Zhang, J.; Shi, W.; Zhang, H.; Huang, C.; Li, J.; Jiang, X.; Zhang, Z. Extraction of density-of-states in amorphous InGaZnO thin-film transistors from temperature stress studies. *Curr. Appl. Phys.* **2014**, *14*, 1713–1717. [CrossRef]
46. Singh, N.; Gupta, R.K.; Lee, P.S. Gold-nanoparticle-functionalized In_2O_3 nanowires as CO gas sensors with a significant enhancement in response. *ACS Appl. Mater. Interfaces* **2011**, *3*, 2246–2252. [CrossRef] [PubMed]
47. Zou, X.; Wang, J.; Liu, X.; Wang, C.; Jiang, Y.; Wang, Y.; Xiao, X.; Ho, J.C.; Li, J.; Jiang, C. Rational design of sub-parts per million specific gas sensors array based on metal nanoparticles decorated nanowire enhancement-mode transistors. *Nano Lett.* **2013**, *13*, 3287–3292. [CrossRef]
48. Kim, S.-J.; Lee, S.-Y.; Lee, Y.-W.; Lee, W.-G.; Yoon, K.-S.; Kwon, J.-Y.; Han, M.-K. Effect of channel layer thickness on characteristics and stability of amorphous hafnium–indium–zinc oxide thin film transistors. *Jpn. J. Appl. Phys.* **2011**, *50*, 024104. [CrossRef]
49. Zhang, H.Z.; Cao, H.T.; Chen, A.H.; Liang, L.Y.; Liu, Z.M.; Wan, Q. Enhancement of electrical performance in In_2O_3 thin-film transistors by improving the densification and surface morphology of channel layers. *Solid-State Electron.* **2010**, *54*, 479–483. [CrossRef]
50. Kannan, P.K.; Saraswathi, R.; Rayappan, J.B.B. CO_2 gas sensing properties of DC reactive magnetron sputtered ZnO thin film. *Ceram. Int.* **2014**, *40*, 13115–13122. [CrossRef]
51. Kang, D.; Lim, H.; Kim, C.; Song, I.; Park, J.; Park, Y.; Chung, J. Amorphous gallium indium zinc oxide thin film transistors: Sensitive to oxygen molecules. *Appl. Phys. Lett.* **2007**, *90*, 192101. [CrossRef]
52. Jeong, J.K.; Won Yang, H.; Jeong, J.H.; Mo, Y.-G.; Kim, H.D. Origin of threshold voltage instability in indium-gallium-zinc oxide thin film transistors. *Appl. Phys. Lett.* **2008**, *93*, 123508. [CrossRef]
53. Jeong, J.; Hong, Y. Debye length and active layer thickness-dependent performance variations of amorphous oxide-based TFTs. *IEEE Trans. Electron Devices* **2012**, *59*, 710–714. [CrossRef]